

# Deflagration-to-Detonation Transition in Unconfined Media

A.Y. Poludnenko<sup>1\*</sup>, T.A. Gardiner<sup>2</sup>, E.S. Oran<sup>1</sup>

<sup>1</sup> Naval Research Laboratory, Washington, DC, USA

<sup>2</sup> Sandia National Laboratories, Albuquerque, NM, USA

## 1 Introduction

Deflagration-to-detonation transition (DDT) can occur in a wide variety of environments ranging from experimental and industrial systems on Earth to astrophysical thermonuclear (type Ia) supernovae explosions. In recent years, substantial progress has been made both experimentally and theoretically in elucidating the nature of this phenomenon in confined systems with walls, obstacles, etc. (see [1] for a detailed review). Shocks in such systems can be formed both by the overall fluid expansion caused by the energy release in the flame, as well as by the repeated interactions of the flame-generated acoustic waves with solid obstacles and with the flame itself. Once a shock of sufficient strength is formed in the system, DDT can occur through a variety of different mechanisms, such as shock collision with an obstacle [2] or shock-flame interactions and the formation of the induction-time gradients [1]. At the same time, it remains unclear whether a subsonic turbulent flame initially present in an unconfined, unpressurized system without pre-existing shocks can undergo DDT and, if such transition is possible, what its mechanism would be.

In this work, we present results of the direct numerical simulations (DNS) of the interaction of high-speed turbulence with premixed flames in a stoichiometric H<sub>2</sub>-air mixture. We demonstrate that at sufficiently high, but subsonic, turbulent velocities, the turbulent flames are inherently unstable and are susceptible to the development of the detonation without assistance of any external shocks or solid boundaries.

## 2 Physical Model and Numerical Method

We model the turbulence-flame interaction using the fixed-grid massively parallel code Athena-RFX [3], the reactive-flow extension of the magnetohydrodynamic code Athena [4]. It employs fully unsplit corner transport upwind scheme which uses PPM spatial reconstruction in conjunction with the HLLC Riemann solver to achieve 3rd-order accuracy in space [4]. The multidimensional coupling and low dissipation properties of this scheme are critical for minimizing numerical inaccuracies such as poor angular-momentum conservation, numerically induced anisotropies, suppression or enhancement of high- $k$  components of the spectrum, etc. Extensive tests of the hydrodynamic solver can be found in [4], and the detailed analysis of the performance of the reactive-flow extensions, including the convergence studies, can be found in [3, 5].

\*Correspondence to: apol@lcp.nrl.navy.mil

Table 1: Reaction Model Parameters and Resulting Laminar Flame Properties

$T_0$	293 K	Initial temperature
$P_0$	$1.01 \times 10^6$ erg/cm <sup>3</sup>	Initial pressure
$\rho_0$	$8.73 \times 10^{-4}$ g/cm <sup>3</sup>	Initial density
$\gamma$	1.17	Adiabatic index
$M$	21 g/mol	Molecular weight
$A$	$6.85 \times 10^{12}$ cm <sup>3</sup> /g·s	Pre-exponential factor
$Q$	46.37 RT <sub>0</sub>	Activation energy
$q$	43.28 RT <sub>0</sub> / M	Chemical energy release
$\kappa_0$	$2.9 \times 10^{-5}$ g/s·cm·K <sup>0.7</sup>	Transport constant
$D_0$	$2.9 \times 10^{-5}$ g/s·cm·K <sup>0.7</sup>	Transport constant
$T_P$	2135 K	Post-flame temperature
$\rho_P$	$1.2 \times 10^{-4}$ g/cm <sup>3</sup>	Post-flame density
$\delta_L$	0.032 cm	Laminar flame thermal width
$S_L$	302 cm/s	Laminar flame speed

We solve the reactive flow equations with thermal conduction, molecular species diffusion, and energy release that control propagation of the laminar flame. The equation of state is that of an ideal gas and the chemical source term describes the first-order Arrhenius kinetics. We consider a stoichiometric H<sub>2</sub>-air mixture with reaction model parameters and the resulting laminar flame properties listed in Table 1 [2].

Turbulence driving is implemented by a spectral method. Fourier transforms of velocity perturbations,  $\delta \mathbf{u}$ , are initialized with random amplitudes and phases with a Gaussian deviation. The desired energy injection spectrum is superimposed on the Fourier transforms of the velocity perturbations. The nonsolenoidal component is projected out to ensure that the resulting perturbations are divergence-free, i.e.,  $\nabla \cdot \delta \mathbf{u} = 0$ . An inverse Fourier transform is performed to obtain the velocity perturbation field in physical space. Resulting velocity perturbations are normalized to ensure the desired total energy injection rate. The method does not induce any large-scale anisotropies and it produces the standard “5/3” slope in the inertial range, even at very low grid resolutions. The saturated value of the kinetic energy density in the system is also insensitive to the resolution. Further description of the turbulence-driving method can be found in [3], and the detailed analysis of the properties of the resulting nonreactive and reactive turbulence is given in [6, 7].

The computational domain is a Cartesian mesh with the size  $256 \times 256 \times 4096$  and an aspect ratio of 16 : 1. The domain width is  $L = 0.518$  cm =  $16\delta_L$  providing the resolution of 16 cells per  $\delta_L$ . It was shown in [3,5] that such resolution is sufficient to obtain an accurate, converged solution. Kinetic energy is injected only at the scale  $L$  to produce a homogeneous, isotropic, Kolmogorov-type turbulence with characteristic velocity  $U = 1.9 \times 10^4$  cm/s =  $63S_L$  at the scale  $L$ . The resulting large-scale eddy turnover time is  $\tau_{ed} = 27.2$   $\mu$ s.

### 3 Results

Figure 1 shows the time evolution of the normalized turbulent flame speed,  $S_T$ , and surface area,  $A_T$ . The  $S_T$  is defined based on the fuel consumption rate. It was shown in [5] that in the thin reaction zone regime, in which small-scale turbulence disrupts the preheat zone of the flame but not the reaction zone,  $A_T$  is

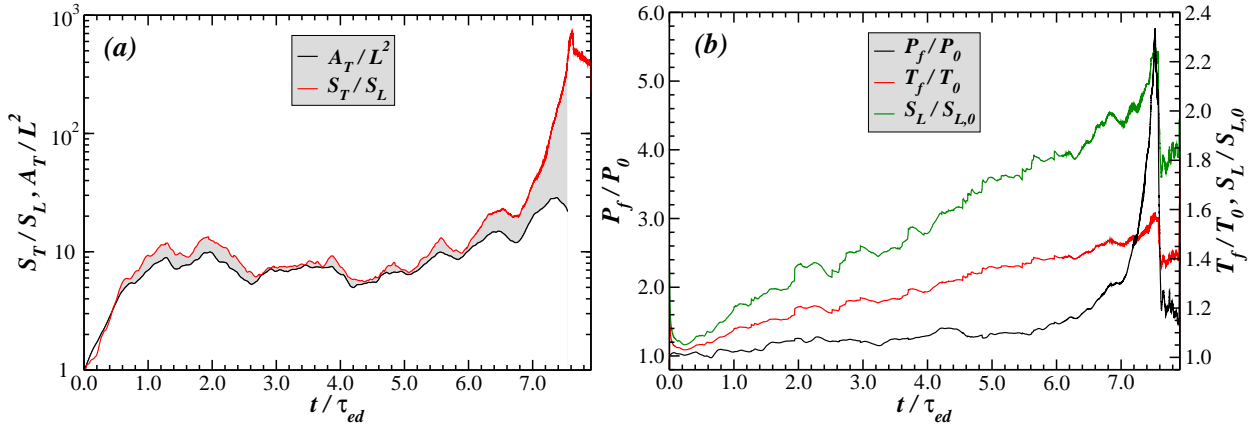


Figure 1: (a) Time evolution of the turbulent flame speed,  $S_T$ , and the flame surface area,  $A_T$ . The  $S_T$  is normalized by the instantaneous values of  $S_L$  shown in panel (b),  $A_T$  is based on the area of the  $Y = 0.15$  isosurface and is normalized by the domain cross-section. Shaded gray area represents burning velocity in excess of what can be attributed to the increase of the flame surface area (see [5]). (b) Time evolution of the average pressure,  $P_f$ , and temperature,  $T_f$ , of pure fuel ( $Y \geq 0.95$ ) contained in the flame brush. Also is shown the laminar flame speed,  $S_L$ , corresponding to the instantaneous values of  $P_f$  and  $T_f$ . All quantities are normalized by their initial values in the domain. Note, that the scale for  $P_f$  is given on the left axis, and for  $T_f$  and  $S_L$  on the right one. See text for further details.

represented by the isosurface of the peak reaction rate. For the reaction model used here, this corresponds to  $Y = 0.15$ .

Dissipation of turbulent energy in the domain causes gradual heating of fuel. As a result, the corresponding laminar flame speed, and, thus, the local burning velocity of the turbulent flame, also increases with time. In order to account for this effect, we record the time evolution of the average pressure,  $P_f$ , and temperature,  $T_f$ , of pure fuel ( $Y \geq 0.15$ ) contained inside the turbulent flame brush. These are shown in Fig. 2b along with the corresponding values of the laminar flame speed,  $S_L$ .

Figure 1a shows that once the turbulent flame reaches the equilibrium after  $t \approx 2\tau_{ed}$ , it enters the quasi-steady state of evolution, which lasts until  $t \approx 6.5\tau_{ed}$ . During this time, turbulent heating increases both  $P_f$  and  $T_f$  isochorically by  $\sim 40\%$  causing an almost two-fold increase of  $S_L$ . The normalized values  $S_T/S_L$  and  $A_T/L^2$  show that during this quasi-steady evolution,  $S_T$  is primarily determined by the increase of the surface area of the turbulent flame. Occasionally, however,  $S_T$  increases by as much as 30% over what can be attributed to the increase in  $A_T$ . The nature of such accelerated burning was studied in [5] and was attributed to the flame collisions and the formation of cusps.

At the time  $t \approx 6.5\tau_{ed}$ , however, burning begins to accelerate substantially. In particular, at this point burning inside the flame brush becomes fast enough to inject on a sound-crossing timescale the amount of energy comparable to the internal energy of the fluid contained inside the flame brush. This causes rapid build-up of pressure inside the flame brush and marks the onset of a catastrophic runaway process.

Figure 2 shows the distributions of pressure and fuel mass fraction, averaged over the domain cross-section, during this runaway. In particular, Fig. 2a shows the development of high pressure inside the flame brush. The pressure distribution is nonuniform and consists of shocks of varying strength moving through the flame

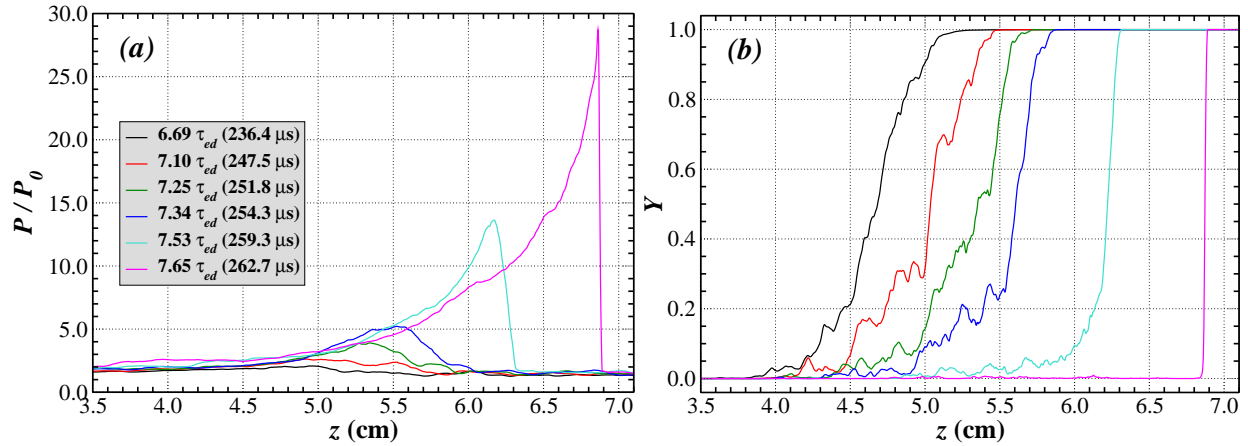


Figure 2: (a) Distributions of normalized pressure,  $P/P_0$ , averaged over the domain cross-section. The time of each profile since ignition is shown in the legend. (b) Distribution of the fuel mass fraction,  $Y$ , averaged over the domain cross-section. Profiles are shown for the same times as in (a). Profiles in cyan correspond to the moment of DDT (cf. Figs. 1b and 3). Note, in both panels only the region of the domain in the vicinity of the flame brush is shown.

brush. As a result, the fuel pressure and temperature grow inside the flame brush grow. This increases the local flame speed, which further accelerates burning, thereby increasing pressure even higher. This creates a positive feedback loop and drives the runaway process.

At this stage, the presence of shock waves inside the flame brush causes the fuel pressure and temperature to be highly nonuniform. In particular, local shock-flame interactions can greatly increase the local flame burning velocity. Consequently, the average laminar flame speed, shown in Fig. 1b and based on  $P_f$  and  $T_f$  averaged over the entire flame brush, becomes a progressively less accurate measure of the actual flame energetics. This causes  $S_T/S_L$  to deviate more and more from  $A_T/L^2$ .

Eventually, shocks of sufficient strength are created such that their collision forms a high-pressure hot spot which ignites a detonation. Emergence of such detonation from the flame brush can be seen in Fig. 3, which also shows the highly nonuniform pressure distribution in the domain. During the DDT, local pressure values in excess of a few hundred atmospheres were observed. The curved shape of the nascent detonation front seen in Fig. 3 is the result of its emergence from a very small region, effectively a point, inside the leading edge of the flame brush. Eventually, it detaches from the flame brush and evolves into a planar detonation wave.

The newly born detonation is initially in the overdriven regime due to the presence of a large region of high pressure behind it. Its initial velocity of  $\approx 2.2 \times 10^5$  cm/s is larger than the CJ velocity of  $1.99 \times 10^5$  cm/s for the reaction model used here [2]. While we do observe the gradual relaxation of the detonation, the length of the computational domain was insufficient to allow it to reach the steady CJ state.

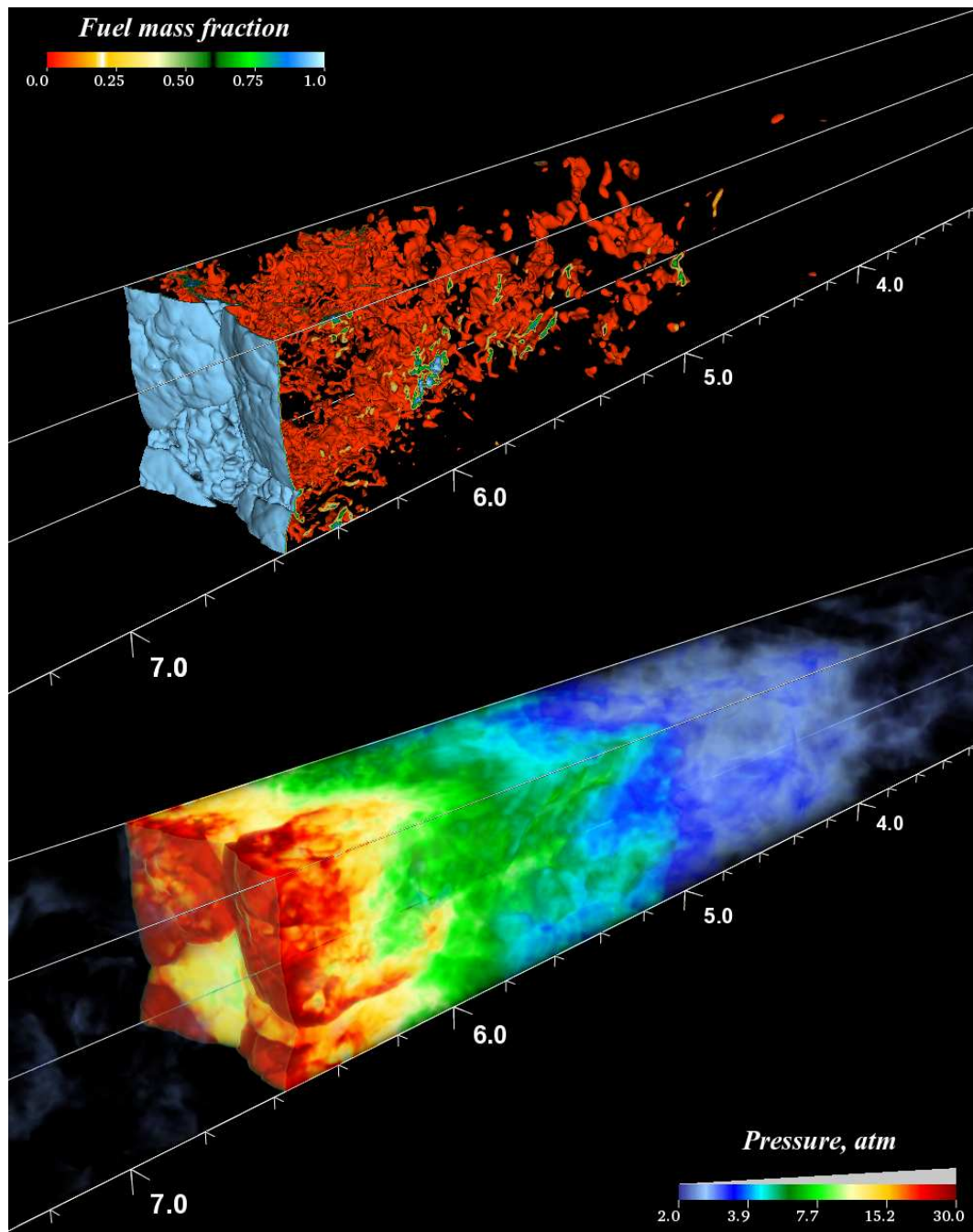


Figure 3: DDT in a high-speed turbulent flame in an unconfined system. *Upper panel:* Structure of the turbulent flame at  $t = 7.59\tau_{ed} = 261 \mu\text{s}$  based on the isovolume of the fuel mass fraction,  $Y$ . Bounding isosurfaces represent  $Y = 0.05$  (blue) and  $Y = 0.95$  (red) and the flame brush is shown from the product side. Curved detonation wave can be seen emerging from the flame brush. *Lower panel:* Corresponding distribution of pressure in the system at the same instant. Note, that colormap is given on a logarithmic scale. In both panels the axis scale shows the distance from the right  $z$ -boundary in cm.

---

**References**

- [1] E.S. Oran, V.N. Gamezo, Origins of the deflagration-to-detonation transition in gas-phase combustion, *Combust. Flame*, 148 (2007) 4-47.
- [2] V.N. Gamezo, T. Ogawa, E.S. Oran, Flame acceleration and DDT in channels with obstacles: Effect of obstacle spacing, *Combust. Flame* 155 (2008) 302-315.
- [3] A.Y. Poludnenko, E.S. Oran, The interaction of high-speed turbulence with flames: Global properties and internal flame structure, *Combust. Flame*, 157 (2010) 995-1011.
- [4] J.M. Stone, T.A. Gardiner, P. Teuben, J.F. Hawley, J.B. Simon, Athena: a New Code for Astrophysical MHD, *Astrophys. J. Supp.* 178 (2008) 137-177.
- [5] A.Y. Poludnenko, E.S. Oran, The interaction of high-speed turbulence with flames: Turbulent Flame Speed, *Combust. Flame*, 158 (2011) 301-326.
- [6] P. Hamlington, A. Poludnenko, E. Oran, Turbulence and scalar gradient dynamics in premixed reacting flows, AIAA-2010-5027, 40th Fluid Dynamics Conference and Exhibit, Chicago, Illinois, June 28-1, 2010.
- [7] P. Hamlington, A. Poludnenko, E. Oran, Intermittency and premixed turbulent reacting flows, AIAA-2011-113, 49th AIAA Aerospace Sciences Meeting including the New Horizons Forum and Aerospace Exposition, Orlando, Florida, Jan. 4-7, 2011.